symmetry

MDPI

Article

Natural Compounds as DPP-4 Inhibitors: 3D-Similarity Search, ADME Toxicity, and Molecular Docking Approaches

Daniela Istrate and Luminita Crisan *

"Coriolan Dragulescu" Institute of Chemistry, 24 M. Viteazu Avenue, 300223 Timisoara, Romania
* Correspondence: lumi_crisan@acad-icht.tm.edu.ro

Abstract: Type 2 diabetes mellitus is one of the most common diseases of the 21st century, caused by a sedentary lifestyle, poor diet, high blood pressure, family history, and obesity. To date, there are no known complete cures for type 2 diabetes. To identify bioactive natural products (NPs) to manage type 2 diabetes, the NPs from the ZINC15 database (ZINC-NPs DB) were screened using a 3D shape similarity search, molecular docking approaches, and ADMETox approaches. Frequently, in silico studies result in asymmetric structures as "hit" molecules. Therefore, the asymmetrical FDA-approved diabetes drugs linagliptin (8-[(3R)-3-aminopiperidin-1-yl]-7-but-2-ynyl-3-methyl-1-[(4-methylquinazolin-2-yl)methyl]purine-2,6-dione), sitagliptin ((3R)-3-amino-1-[3-(trifluoromethyl)-6,8-dihydro-5H-[1,2,4]triazolo[4,3-a]pyrazin-7-yl]-4-(2,4,5-trifluorophenyl)butan-1-one), and alogliptin (2-[[6-[(3R)-3-aminopiperidin-1-yl]-3-methyl-2,4-dioxopyrimidin-1-yl]methyl]benzonitrile) were used as queries to virtually screen the ZINC-NPs DB and detect novel potential dipeptidyl peptidase-4 (DPP-4) inhibitors. The most promising NPs, characterized by the best sets of similarity and ADMETox features, were used during the molecular docking stage. The results highlight that 11 asymmetrical NPs out of 224,205 NPs are potential DPP-4 candidates from natural sources and deserve consideration for further in vitro/in vivo tests.

Keywords: diabetes; ZINC-NPs DB; 3D shape similarity search; molecular docking

Citation: Istrate, D.; Crisan, L. Natural Compounds as DPP-4 Inhibitors: 3D-Similarity Search, ADME Toxicity, and Molecular Docking Approaches. *Symmetry* **2022**, *14*, 1842. https://doi.org/10.3390/sym14091842

Academic Editors: György Keglevich and Jan Cz. Dobrowolski

Received: 11 July 2022
Accepted: 2 September 2022
Published: 5 September 2022

1. Introduction

Diabetes mellitus (DM) is a complex, fast-growing chronic metabolic disorder around the world. The World Health Organization (WHO) reports that 442 million people worldwide have diabetes [1], and International Diabetes Federation (IDF) has announced that 537 million adults aged between 20 and 79 years old live with diabetes, of which 61 million are in Europe. Worldwide, every five seconds, there is a death caused by diabetes [2]. At the end of 2021, 6.7 million deaths were reported. Two main types of DM are known: type 1 (T1DM), also known as insulin-dependent diabetes mellitus (IDDM), and type 2 (T2DM), also known as non-insulin-dependent diabetes mellitus (NIDDM) [3]. In addition, a new type of diabetes, named gestational diabetes, has been reported in pregnant women with hyperglycemia [4]. Patients with T2DM represent over 90% of diabetes cases [5]. In the last few decades, cases of type 2 diabetes have increased dramatically, and the estimation of the IDF for 2030 and 2045 is 643 and 783 million people with diabetes, respectively [2]. Hence, identifying bioactive compounds for T2DM management and treatment is a continuous challenge [6,7]. Since the 2000s, the class of gliptins, as dipeptidyl peptidase-4 (DPP-4) inhibitors, [8–10] has become of interest to the scientific community because it is involved in improvements of glycemic control (without causing hypoglycemia) and, at the same time, is very well tolerated [11,12]. For adults, the first drug of the gliptin class approved by the FDA (October 2006) as a DPP-4 inhibitor, used in the management of T2MD, was sitagliptin (Figure 1) [13]. Many treatment tests have exhibited a good efficacy of sitagliptin by improving glycemic control in those suffering from T2DM [14]. In 2008, the European Medicines Agency (EMA) approved vildagliptin [15] for the treatment of T2MD as monotherapy or in

combination with metformin. In July 2009, May 2011, and January 2013, the FDA approved three new DPP-4 inhibitors to fight T2DM, named saxagliptin [16], linagliptin [17], and alogliptin [18] (Figure 1). Linagliptin [19,20] and alogliptin [21,22] are considered highly selective inhibitors that offer a potent inhibition for DPP-4 when used either alone or in conjunction with other anti-diabetic drugs (e.g., metformin) [23,24]. According to different investigational stages, numerous structures such as anagliptin [25], gemigliptin [26], teneligliptin [27], evogliptin [28], omarigliptin [29], trelagliptin [30], and gosogliptin [31] are expected to be annotated. During the treatment with different gliptins, several side effects, such as pancreatitis, some kidney problems, hypersensitivity, etc., were observed. Therefore, there is a need to find new DPP-4 inhibitors with improved pharmacological profiles. Over the past few years, in silico techniques (Quantitative Structure–Activity Relationship (QSAR) [32–35], ligand-based and structure-based virtual screening [36,37], pharmacophore modeling [7,38,39], molecular docking [40–42], semiempirical/DFT calculations [43–46], molecular dynamics simulation [47,48], etc.) have been widely used in the early phase of drug discovery due to their efficiency and low costs. Strategies for these techniques can vary significantly depending on the availability of the target and ligand information. The major advantages of them are: (i) they are very fast but depend on both hardware and software components, (ii) they allow the optimization and identification of new "hits", and (iii) they eliminate compounds with undesirable physicochemical and pharmacodynamic properties. In this light, in the present work, we exemplify a virtual screening workflow involving 3D-shape similarity searches, followed by molecular docking techniques and ADMET predictions, to identify novel NPs as potential DPP-4 inhibitors that could be used in the management of T2DM. Nowadays, the management and prevention of T2DM are big challenges; the aim is to control the complications (damage to the nerves, cardiovascular, kidneys, bone fragility, etc.) caused by DM and to sustain quality of life.

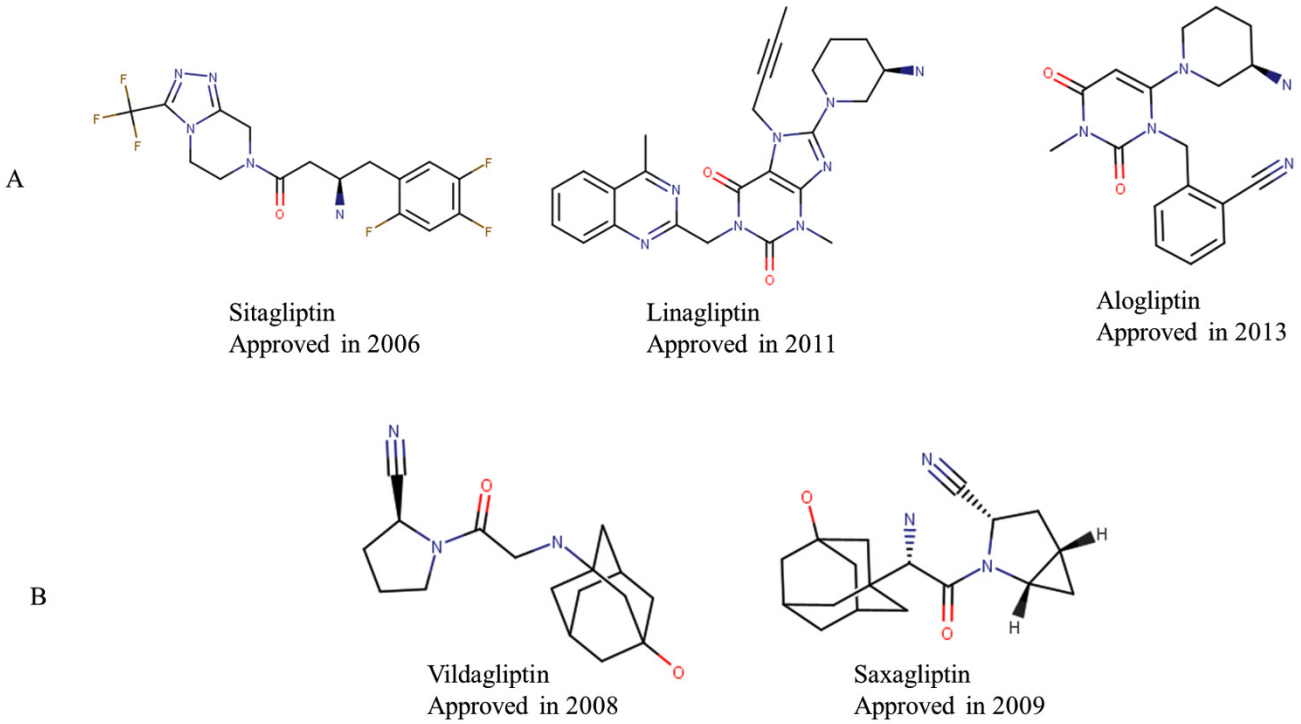

Figure 1. The chemical structure of asymmetrical T2DM FDA-approved drugs: (**A**) non-peptidomimetics and (**B**) peptidomimetics.

2. Materials and Methods

In order to achieve our goals, the 3D-shape similarity and molecular docking studies were performed using Rapid Overlay of Chemical Structures (ROCS) [49] and Fast Rigid Exhaustive Docking (FRED) [50] tools from the OpenEye package (https://www.eyesopen.com/). The crystal structures of human DPP-4 (PDB ID: 1X70, 2RGU, 2ONC, 3W2T, and 3BJM) connected to FDA-approved drugs (sitagliptin, linagliptin, alogliptin, vildagliptin, and saxagliptin) were downloaded from the RCSB Protein Data Bank (PDB) (https://www.rcsb.org, accessed on 14 April 2022). A BIOVIA Studio visualizer [51] was employed for the visual check of the shape superposition and binding interactions. Additionally, the physicochemical and pharmacokinetic properties were calculated with the help of the SwissADME [52] (http://www.swissadme.ch/, accessed on 10 May 2022) and pkCSM [53] (http://biosig.unimelb.edu.au/pkcsm/, accessed on 10 May 2022) online tools.

2.1. Data Set

Natural products (NPs) have been deemed the source of the most used active components in medicine. Nowadays, the positive effects of NPs or their derivatives are mentioned in the treatment of various types of diabetes, cardiovascular diseases, viral diseases, or even cancers. The 224,205 natural products of the ZINC-NPs DB [54] were downloaded from http://zinc15.docking.org/ (accessed on 8 January 2021) and further prepared [55] for analysis using the LigPrep module [56] of the Schrödinger suite and Omega [57] from the OpenEye package. The T2DM FDA-approved drugs: peptidomimetics (vildagliptin, saxagliptin) and non-peptidomimetics (sitagliptin, alogliptin, and linagliptin) (Figure 1), high selective DPP-4 inhibitors, were investigated. For the 3D-shape similarity search and molecular docking approaches, peptidomimetics drugs were eliminated due to their covalent bonds with the Ser630 residues of receptors (3W2T and 3BJM) that cannot be reproduced with FRED software.

2.2. Shape-Based Similarity Search in a Chemical Database

ROCS is a recognized and widely used shape comparison application based on the principle that similar molecules are those whose volumes overlap very well. For ROCS analysis, the co-crystalized conformations of the ligands extracted from the crystal structure of human DPP-4 were engaged as query molecules (Figures 1 and 2). For the 3D-shape similarity search, Shape Tanimoto (ShT) (Equation (1)), Tanimoto Combo (TC), and Combo Score (CS) as significant metric parameters were calculated between query molecules and each of the 224,205 NPs from the ZINC-NPs DB. The ShT parameter includes shape alone and has a value between 0 and 1, TC comprises both shape fit and color (Shape Tanimoto is added to the Color Tanimoto) and has a value between 0 and 2, and CS contains both shape fit and color (Shape Tanimoto is added to the Scaled Color) and has a value between 0 and 2.

$$ShT = \frac{V_{XY}}{V_{XX} + V_{YY} - V_{XY}} \quad (1)$$

where

V_{XX} and V_{YY} are the self-overlap volumes of molecules X and Y;
V_{XY} is the overlap volume between molecules X and Y.

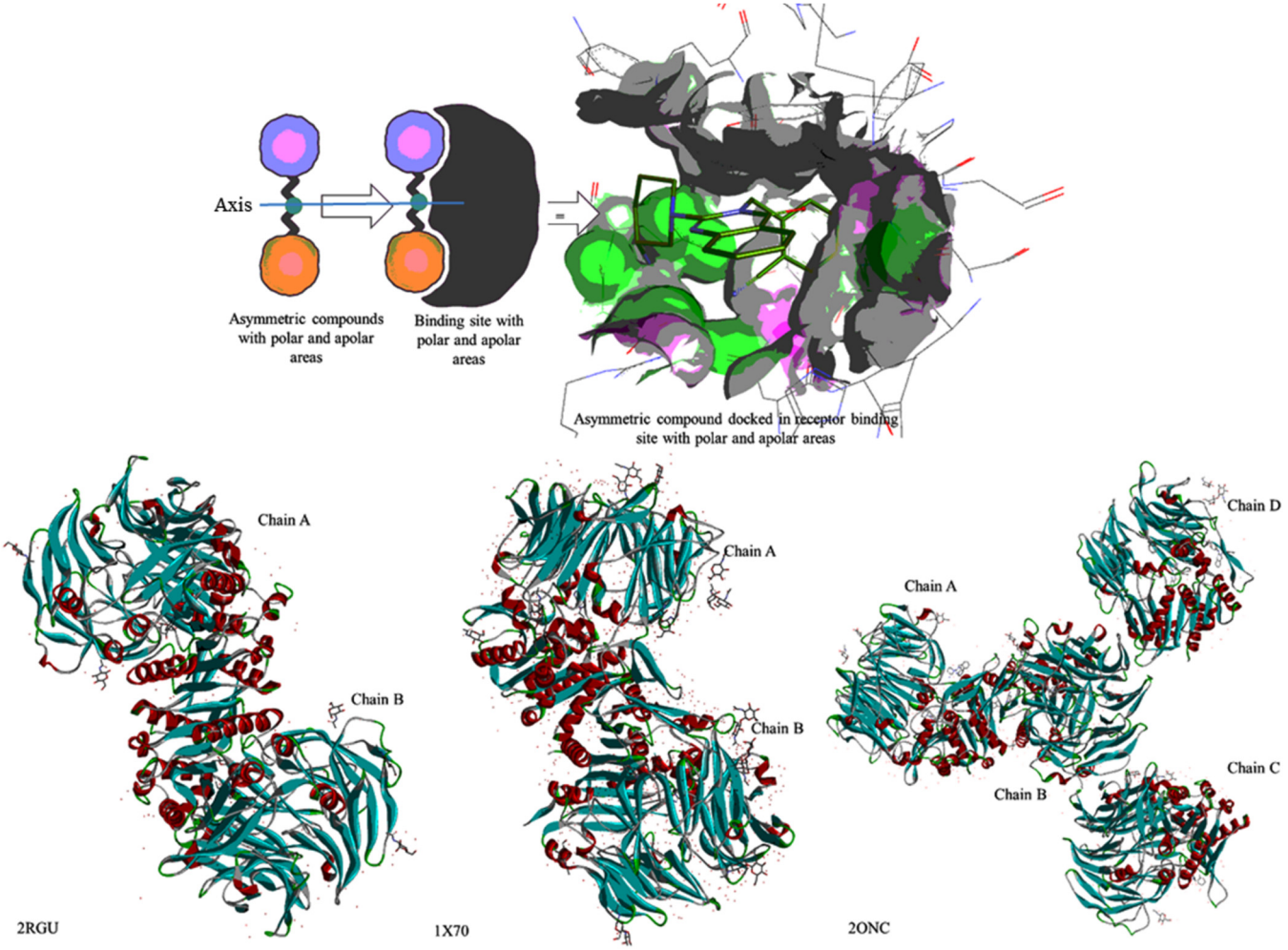

Figure 2. Schematic representation of DPP-4 X-ray crystal structures.

2.3. Docking Study

The asymmetric positions of the RX crystallographic structures are the result of several factors: (i) dimerization, (ii) crystal packing, (iii) flexibility, and (iv) ligand binding [58,59]. As the first step of our study, the X-ray crystal structures of DPP-4 in complex with sitagliptin (PDB ID: 1X70) [60], linagliptin (PDB ID: 2RGU) [61], and alogliptin (PDB ID: 2ONC) [62] were downloaded from RCSB PDB and analyzed. In RCSB PDB, 2RGU and 1X70 are crystallized as dimers with two chains (A and B), and 2ONC is crystallized as a tetramer with four chains (A, B, C, and D). For all three X-ray crystal structures, chain A was selected for further analysis (Figures 2 and 3).

For receptor preparation and refinement, the MakeReceptor [63] module from the OpenEye package step was engaged. The conformations of NPs prepared for the 3D-shape analysis stage were further utilized in the rigid docking investigation. Rigid ligand docking protocol using FRED [50] of the OpenEye suite was applied for predicting DPP-4–NPs binding modes and to rank-order NPs based on the Chemgauss4 scoring function (CG4). Ten poses for each NP were generated, and the best one was selected by considering its ligand–target interactions and CG4 docking scores. The molecular docking simulation was confirmed by (i) re-docking the X-ray ligand structure onto its binding site and (ii) the RMSD (root mean square deviation) calculation between the re-docked X-ray ligand structure and its co-crystallized structure, employing the Maestro module of Schrödinger [64].

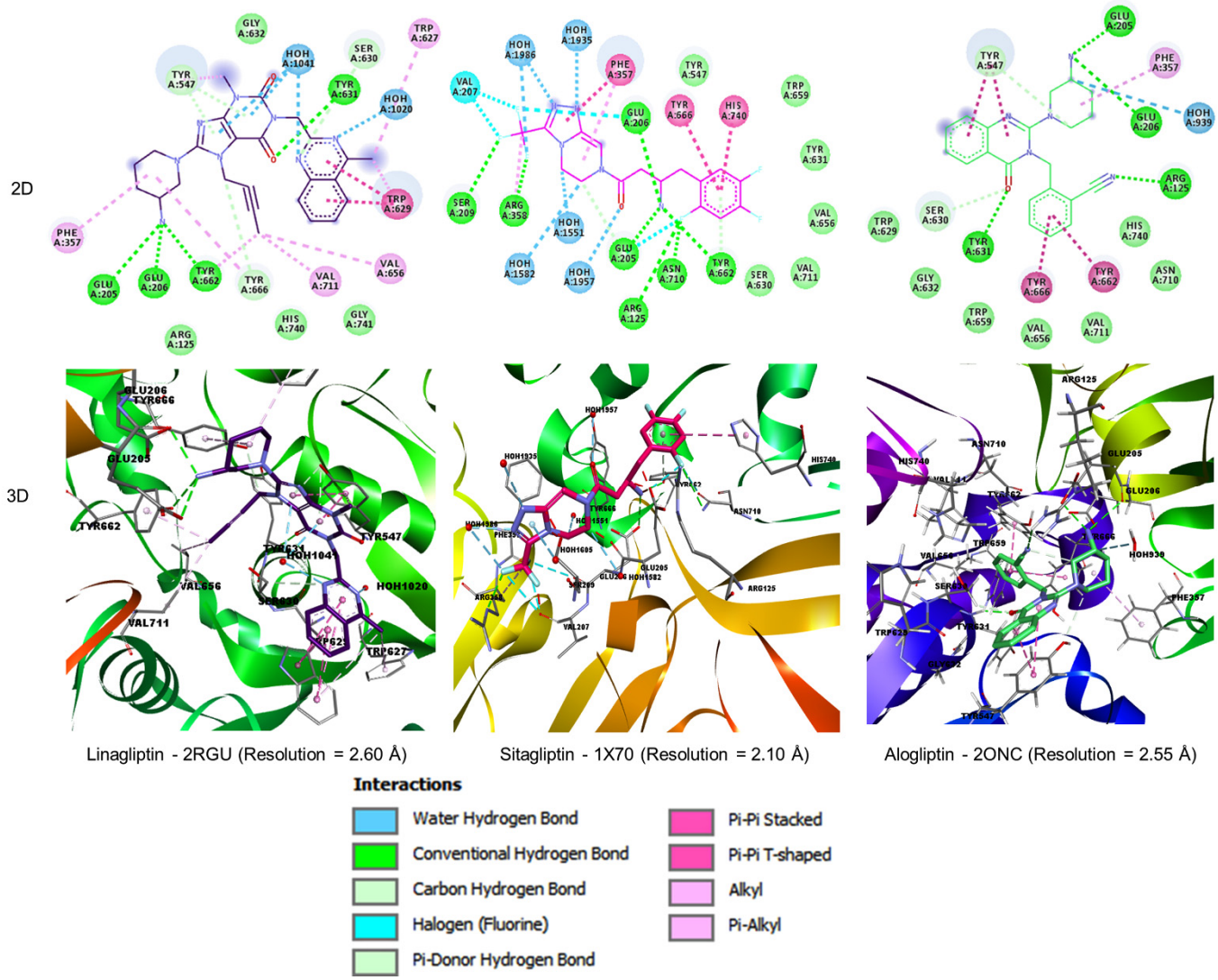

Figure 3. The approved drugs (linagliptin, sitagliptin, and alogliptin) in the 2RGU, 1X70, and 2ONC binding sites (2D and 3D presentation). To facilitate the visualization, only essential amino acids implicated in interactions with RX ligands are shown.

2.4. Bioavailability and In Silico ADME/T Screening for Drug-Likeness

The physicochemical and pharmacokinetic properties of T2DM FDA-approved drugs and selected NPs were predicted using the pkCSM [53] and SwissADME [52] online tools. The oral bioavailability properties were analyzed using Lipinski's 'Rule of Five' [65]. The rule is constructed on the observation that approved drugs have a molecular weight of a maximum of 500, 10, or fewer hydrogen bond acceptor sites, 5 or fewer hydrogen bond donor sites, and a LogP no higher than 5 [66]. Moreover, the absorption, distribution, metabolism, excretion, and toxicity (ADME/T) properties prediction with pkCSM can help us to prioritize, from a theoretical point of view, a compound as a drug candidate. Furthermore, passive human gastrointestinal absorption (HIA) and blood–brain barrier (BBB) permeation, as well as the rapid assessment of drug-likeness, were predicted using BOILED-Egg and Bioavailability Radar, available on the SwissAdme platform.

3. Results

The workflow scheme (Figure 4) followed in this paper involves (1) a 3D-similarity search, applying three FDA-approved drugs and the ZINC-NPs DB of 224,205 NPs; (2) a molecular docking investigation, (3) ADMETox, and (4) an investigation of the results.

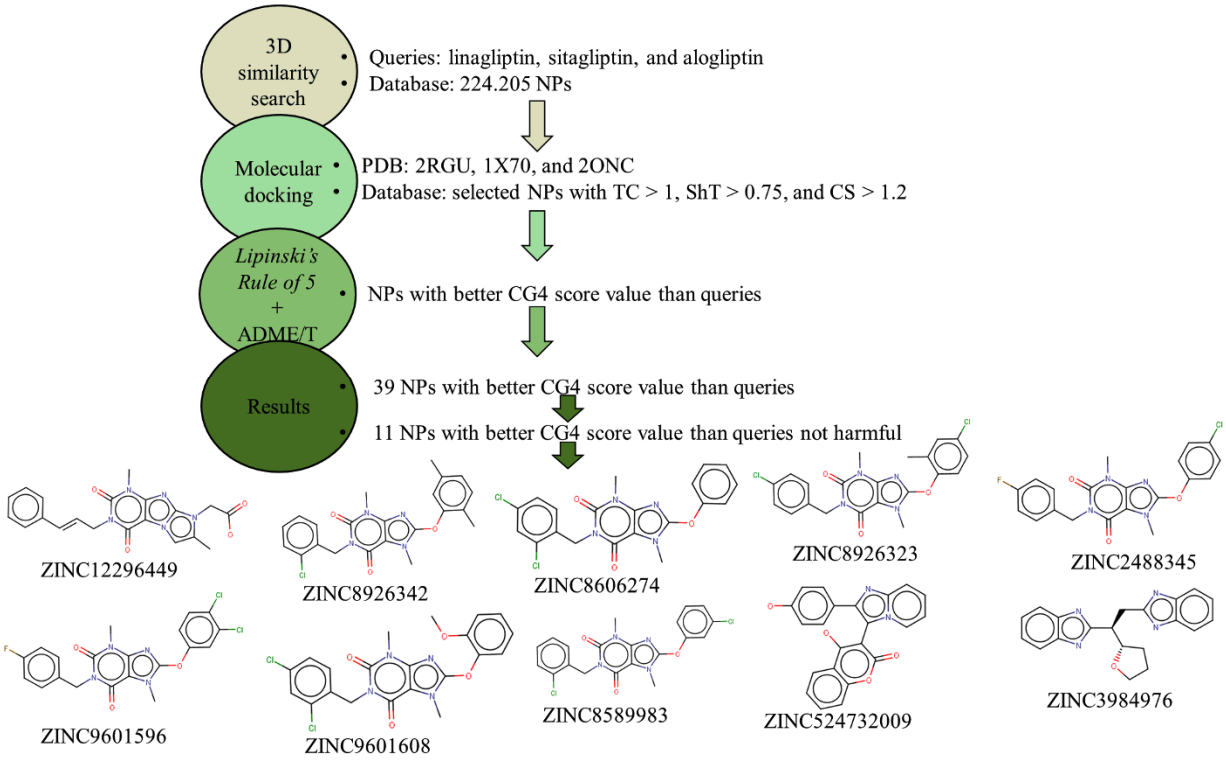

Figure 4. Workflow scheme.

The ROCS similarity analysis (Figure 5a–c) between the query molecules (linagliptin, sitagliptin, and alogliptin) and the screened ZINC-NPs DB suggests that: (1) 218 NPs display TC > 1, 81 display ShT > 0.75, and 65 display CS > 1.2 towards linagliptin; (2) 848 NPs display TC > 1, 1036 display ShT > 0.75, and 632 display CS > 1.2 towards sitagliptin; and (3) 2178 NPs display TC > 1, 1152 display ShT > 0.75, and 1404 display CS > 1.2 towards alogliptin. Of these, 35 NPs linked to linagliptin, 147 NPs related to sitagliptin, and 505 NPs connected to alogliptin satisfied all three criteria of TC > 1, ShT > 0.75, and CS > 1.2 (Tables S1–S3, Figure 5d–f).

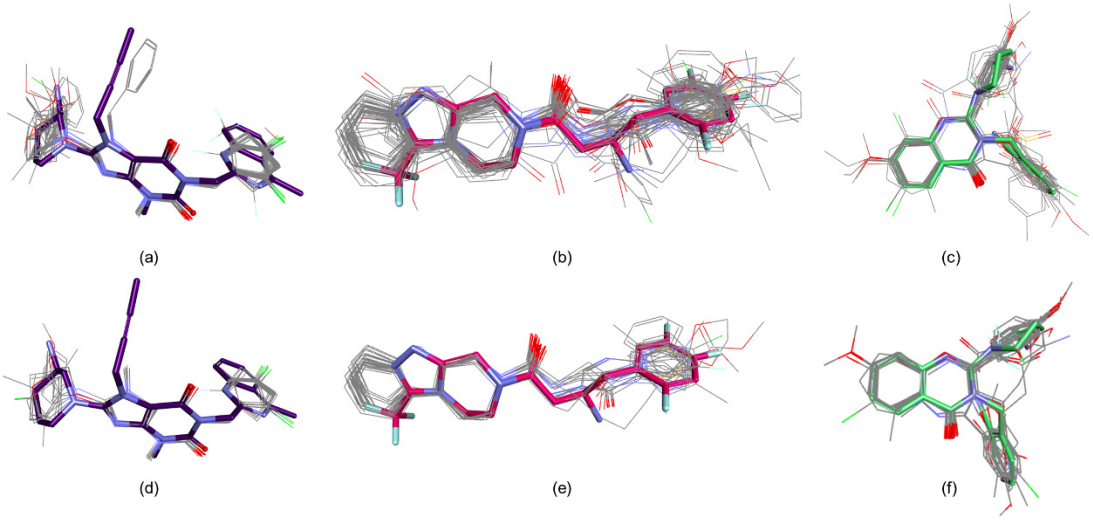

Figure 5. The first fifty NPs according to the TC value overlaid on linagliptin (**a**), sitagliptin (**b**), and alogliptin (**c**), and the first twenty NPs with 3D similarity coefficients of TC > 1, ShT > 0.75, and CS > 1.2, overlaid on linagliptin (**d**), sitagliptin (**e**), and alogliptin (**f**). The RX ligands are shown as sticks and the selected NPs as lines.

NPs that simultaneously met all three similarity criteria (Tables S1–S3) were included in molecular docking studies. The X-ray structures of the DPP-4 receptors co-crystallized with linagliptin (PDB ID: 2RGU, resolution: 2.60 Å) [61], sitagliptin (PDB ID: 1X70, resolution: 2.10 Å) [60], and alogliptin (PDB ID: 2ONC, resolution: 2.55 Å) [62] were prepared for docking by generating the actives sites with the outer contour of 495 $Å^3$, 650 $Å^3$, and 735 $Å^3$, respectively, using the MakeReceptor [63] module from the OpenEye suite with default options. As asymmetrical molecules demand a comparatively large receptor binding site or one with both polar and non-polar regions, the box volumes were set to 7114 $Å^3$ for 2RGU, 5029 $Å^3$ for 1X70, and 5716 $Å^3$ for 2ONC. For each of the three receptors, the water molecules involved in hydrogen bondings were preserved (Figure 3). The accuracy of the docking protocol was checked by re-docking the co-crystallized ligands, linagliptin, sitagliptin, and alogliptin into the active pockets of DPP-4 (2RGU, 1X70, and 2ONC, respectively). Re-docking processes of the co-crystallized ligands showed the efficiency and validity of the docking experiments through RMSD values of 1.076 between the re-docked poses of linagliptin and the native ones (Figure 6a), 1.056 between the re-docked poses of sitagliptin and the native ones (Figure 6b), and 0.388 between the re-docked poses of alogliptin and the native ones (Figure 6c).

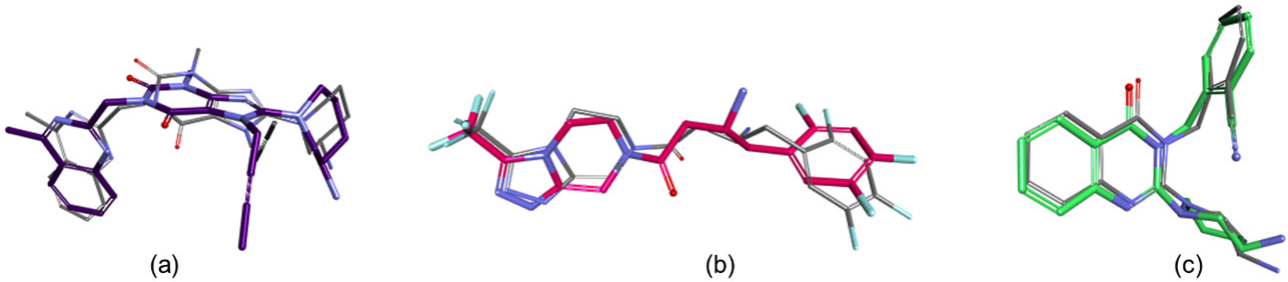

Figure 6. The best re-docked pose (grey) of linagliptin and the co-crystallized (purple) one (**a**), the best re-docked pose of sitagliptin (grey) and the co-crystallized (magenta) one (**b**), and the best re-docked pose (grey) of alogliptin and the co-crystallized (green) one (**c**).

The good validation of the docking procedure allowed us to perform molecular studies on the selected NPs to predict their binding modes and to rank-order them based on the Chemgauss4 (CG4) scoring function (Tables 1 and S4–S8). Next, a visual inspection of the 2D- and 3D-binding interactions of the docked conformations was performed using BIOVIA Discovery Studio [51]. The molecular docking analysis results revealed that thirty-two NPs had the most favorable docking CG4 scores of −8.931 to −4.550 compared to −4.460 for linagliptin; five NPs had the most favorable docking CG4 scores of –10.551 to −9.138 compared to −8.859 for sitagliptin; and five NPs had the most favorable docking CG4 scores of −11.613 to −10.850 compared to −10.635 for alogliptin (Table S4). These results indicate that the predicted NPs might have better inhibitory activity against DPP-4. To estimate the safety and efficacy of selected NPs, physicochemical, pharmacokinetic, and pharmacodynamic profiles were analyzed to predict their potential use in drug development (Tables S5–S8). In the first step, the physicochemical properties and drug-likeness results are checked (Table 1). The selected NPs displayed MW values less than 500 Da (MW = 290.36 ÷ 478.40), logP values less than 5 (logP = 0.95 ÷ 4.24), and HBA values less than 10 (with three exceptions: HBA = 11 for ZINC33833796 and ZINC85509222, and HBA = 12 for ZINC84153787) (HBA = 1 ÷ 12), HBD less than 5 (HBD = 0 ÷ 7), and TPSA less than 140 Å (TPSA = 41.03 Å ÷ 199.51 Å). These results show that the selected NPs are very likely to be orally active, except for ZINC84153787, ZINC33833796, and ZINC85509222, with two violations for the Lipinski rules, and ZINC33833997, with one violation for the Lipinski rules (Table 1). These compounds were removed from further analysis. Moreover, Bioavailability Radar (Figure 7), generated with the SwissAdme platform, illustrates that except for INSATU, all predicted properties of the selected NPs are

located in the pink area (LIPO, lipophilicity (XLOGP3 = 0.7 ÷ 5.0), SIZE, molecular weight (MW = 150 ÷ 500 g/mol), POLAR, polarity (TPSA = 20 ÷ 130 Å^2), INSOLU, insolubility (log S < 6), INSATU, insaturation (fraction of carbons in the sp3 hybridization > 0.25), and FLEX, flexibility (RBN < 9) and, thereby, support the NPs' orally bioavailable character.

Table 1. Physicochemical properties and drug-likeness results for selected NPs.

NPs ID	CG4	MW	HBA	HBD	RBN	TPSA	LogP	Lipinski #Violations
ZINC84153787	−8.931	478.40	***12***	***7***	5	***199.51***	2.11	2
ZINC33833997	−8.354	432.38	***10***	***6***	4	***170.05***	1.71	1
ZINC33833796	−8.209	446.36	***11***	***6***	4	***187.12***	1.15	2
ZINC8926342	−6.555	424.88	4	0	4	71.05	3.94	0
ZINC12296449	−6.354	393.40	5	1	5	103.53	2.98	0
ZINC8606274	−6.350	431.27	4	0	4	71.05	3.94	0
ZINC9601609	−6.208	445.30	4	0	4	71.05	4.24	0
ZINC8926323	−6.177	475.72	4	0	4	71.05	3.97	0
ZINC2488345	−6.005	414.82	5	0	4	71.05	3.75	0
ZINC9601596	−5.765	449.26	5	0	4	71.05	3.98	0
ZINC1094329	−5.719	436.33	3	0	3	65.06	4.07	0
ZINC8916385	−5.618	422.31	3	0	3	65.06	3.87	0
ZINC640985	−5.496	377.83	4	1	5	85.29	3.29	0
ZINC832612	−5.467	432.31	3	0	3	65.06	3.77	0
ZINC2334127	−5.462	446.34	3	0	3	65.06	3.88	0
ZINC838204	−5.433	377.83	4	2	5	94.08	2.98	0
ZINC838200	−5.433	377.83	4	2	5	94.08	3.00	0
ZINC6732655	−5.428	410.30	3	1	6	73.85	3.83	0
ZINC9601608	−5.385	461.30	5	0	5	80.28	4.09	0
ZINC838142	−5.353	385.44	4	0	3	65.06	3.70	0
ZINC1108640	−5.265	410.30	3	1	5	73.85	3.73	0
ZINC2488364	−5.058	377.83	4	1	6	83.08	3.40	0
ZINC9601615	−5.012	436.30	4	1	7	83.08	3.66	0
ZINC4147162	−4.938	420.30	3	1	6	73.85	3.73	0
ZINC1094334	−4.890	389.84	4	0	3	74.29	3.49	0
ZINC2488384	−4.883	422.28	4	1	6	83.08	3.58	0
ZINC789645	−4.880	371.41	4	0	3	65.06	3.62	0
ZINC8589983	−4.865	431.27	4	0	4	71.05	3.76	0
ZINC13512682	−4.767	412.27	4	1	6	83.08	3.60	0
ZINC13142224	−4.745	387.43	5	1	8	92.31	3.58	0
ZINC6565526	−4.550	407.83	5	0	3	74.29	3.27	0
Linagliptin	−4.460	472.54	6	1	4	116.86	3.73	0
ZINC2508009	−10.551	290.36	2	2	4	55.12	2.44	0
ZINC85879571	−9.829	321.38	3	2	4	73.91	1.92	0
ZINC11692316	−9.682	363.41	3	3	4	85.43	1.81	0
ZINC96112842	−9.297	307.37	5	1	5	81.60	1.52	0
ZINC604405970	−9.149	335.44	1	1	6	41.03	3.10	0
ZINC12296782	−9.138	326.39	2	2	2	68.44	2.72	0
Sitagliptin	−8.859	407.31	10	1	4	77.04	2.35	0
ZINC15674091	−11.613	360.41	5	2	4	78.18	2.58	0
ZINC524732009	−11.498	370.36	5	2	2	87.97	2.50	0
ZINC15830055	−11.158	365.47	5	3	3	68.09	3.47	0
ZINC3984976	−11.003	332.40	3	2	4	66.59	2.60	0
ZINC85509222	−10.850	450.39	***11***	***7***	3	***186.37***	0.95	2
Alogliptin	−10.635	339.39	4	1	3	97.05	2.38	0

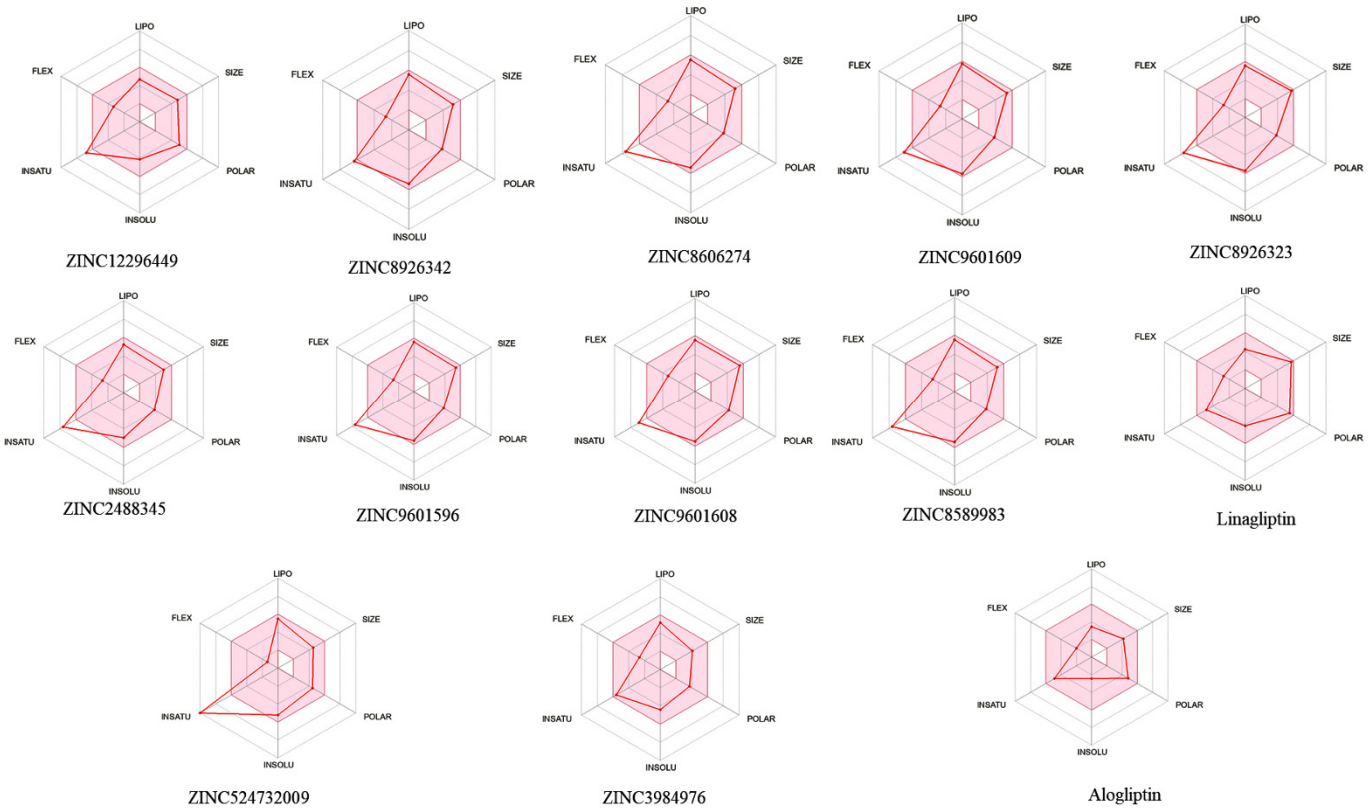

Figure 7. Bioavailability Radar (for a good visualization, only the final eleven NPs and their query drugs are represented, see below).

The high water solubility observed for selected asymmetrical NPs raises the probability of a significant number of interactions with the DPP-4 binding site and, in the same manner, permits them to be largely distributed in the cellular medium (intra and extra) and to penetrate biological membranes.

In the next step, the pharmacokinetic properties and toxicity were calculated and analyzed (Tables S5–S8). The predicted absorption parameters (Table S5) of Caco-2 (membrane permeability indicated by colon cancer cell line), intestinal absorption, P-glycoprotein (Pgp) substrate or inhibitor, and skin permeability levels show that only ten of thirty-nine NPs displayed high Caco-2 cell permeability (Caco-2 > 0.90); all thirty-nine NPs indicate a good intestinal absorption and skin permeability (HIA > 30%, and logKp > −2.5), twenty NPs could be a substrate of Pgp, and fifteen and thirteen NPs are likely to be P-glycoprotein I and II inhibitors. The predicted distribution parameters (Table S6) of VDss (volume of distribution), BBB (brain–blood barrier) permeability, and CNS (central nervous system) permeability show that twelve NPs are highly distributed (logVDss > 0.45), two NPs are considered to be able to easily cross the BBB (logBB > 0.3), and twenty-nine NPs are considered to be able to penetrate the CNS (logPS > −2). In addition, BOILED-Egg from SwissADME, illustrated in Figure 8, shows the human intestinal absorption (HIA) and the brain access/penetration of NPs and the approved drug molecules by plotting the graph WLOGP versus TPSA. The NPs situated in the white area and the yellow region (yolk) present the highest expectation of being absorbed by the human gastrointestinal tract and the highest chance of brain penetration, respectively. Furthermore, the NPs marked with red and blue dots are supposed to be non-efflux from the CNS by Pgp (Pgp− (non-substrates)) or efflux from the CNS by Pgp (Pgp+ (substrates)). The inhibitory or substrate behavior of the cytochrome P450 enzymes (CYPs) was verified for all selected NPs. The metabolism parameters based on the CYP models for substrate (CYP2D6, CYP3A4) or inhibition (CYP1A2, CYP2C19, CYP2C9, CYP2D6, and CYP3A4) are presented in Table S7. The excretion parameters (total clearance and renal organic cation transporter (OCT2) sub-

strate) show that twenty-one NPs have good renal clearance. The hepatotoxicity parameter (Table S8) indicates that twenty-eight out thirty-nine NPs could be harmful. The remaining eleven NPs, predicted (Figures 8–10) as non-harmful, were subject to further investigation. Among these eleven selected NPs, ten NPs possibly do not inhibit the hERG (human ether-a-go-go-related gene) channel and may not have cardiotoxicity. Skin sensitization was not observed for any of the eleven predicted NPs.

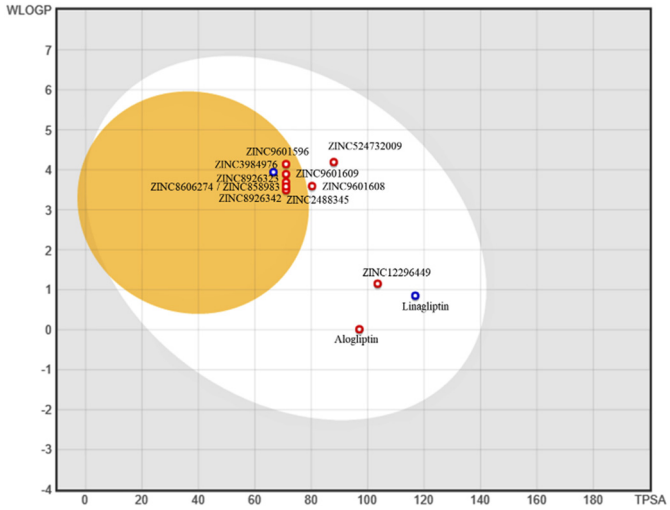

Figure 8. Boiled-EGG (WLOGP vs. TPSA) for the predicted NPs and approved drugs (for a good visualization, only the final eleven NPs and their query drugs are represented).

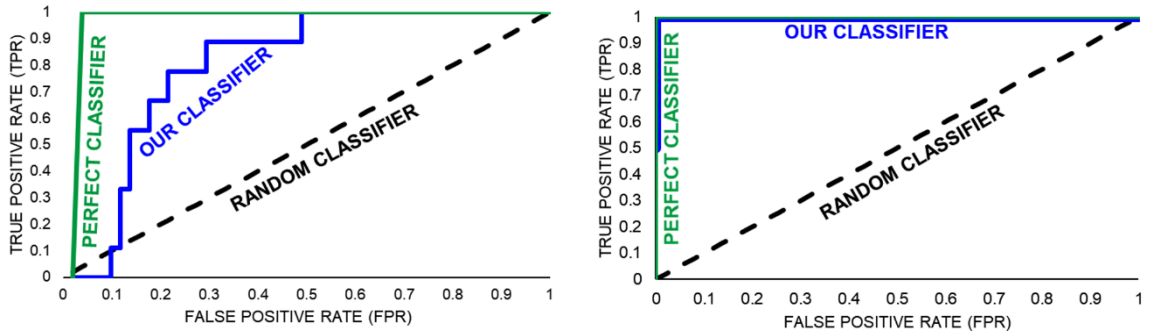

Figure 9. ROC curve for NPs vs. generated decoys in the 2RGU binding site (**a**) and for NPs vs. generated decoys in the 2ONC binding site (**b**). TPR represents the fraction of correctly predicted actives; FPR indicates the ratio of the mispredicted inactives.

Retrospective validation of in silico protocol and retrieval of "hits" in terms of the area under curve (AUC) metric [67] was assessed using the in-house developed program ETICI1.6 (Evaluation Tool In ChemInformatics) [68]; 50 decoys were generated [69,70] for each query molecule and were prepared for docking using the same protocol as the dataset. In the next step, the rank order of the decoys was evaluated considering their CG4 docking scores in relation to the selected NPs. The results show significant values for the AUC parameter. The AUC value of 0.802 (±0.059) for 2RGU provides a very good number of NPs recovered at the top of the list, and the AUC value of 1.000 (±0.000) for 2ONC shows the perfect separation of the selected NPs at the top of the ranking list. In addition, the early enrichment [71] step was involved in order to prove the performance of the in silico protocol. The receiver operating characteristics (ROC) curve (Figure 9) is depicted by involving the two parameters of true positive rate (TPR) and false positive rate

(FPR). The black line illustrates a random classifier, the green line shows a perfect classifier, and the blue line indicates the classifier results for our protocol.

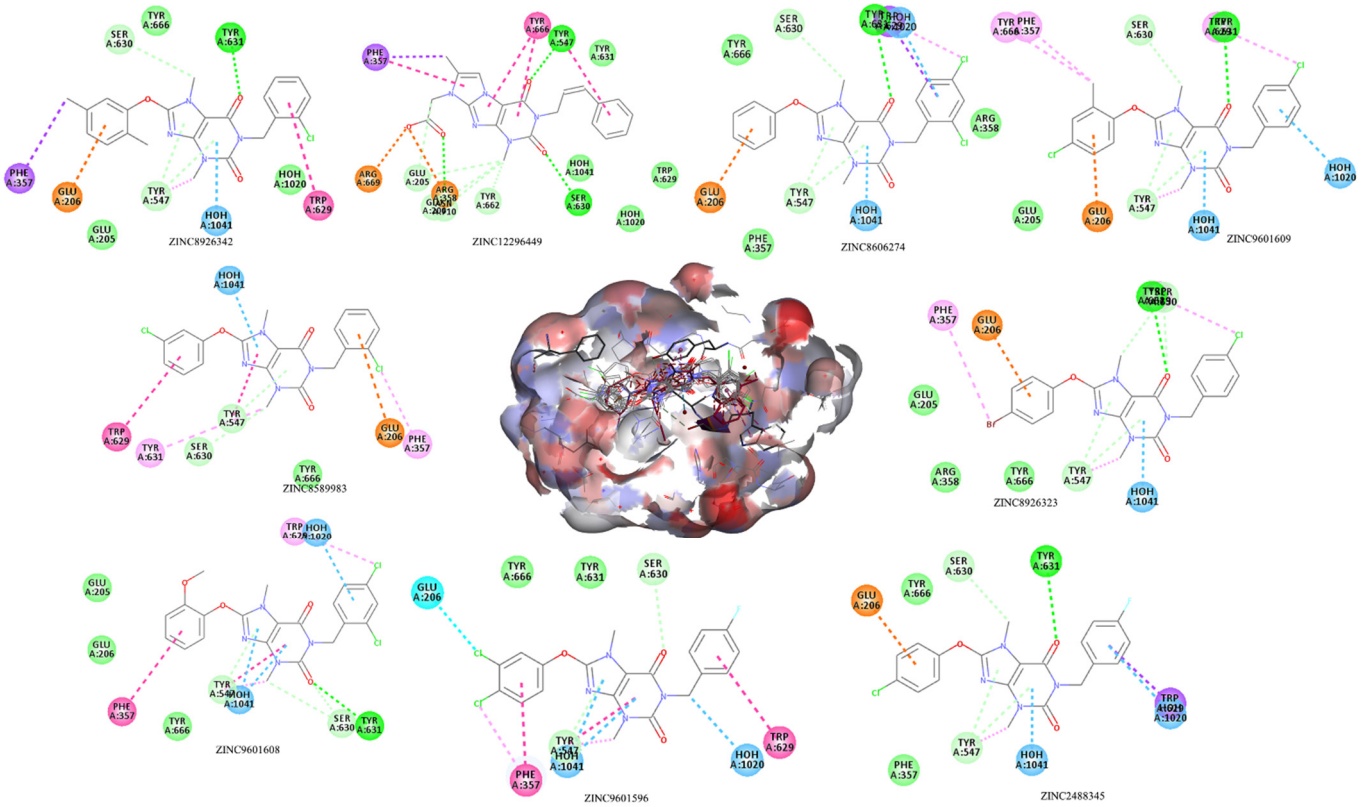

Figure 10. The nine docked NPs in the 2RGU active sites, showing CG4 scores better than linagliptin. Polar and non-polar regions of the binding site of 2RGU are illustrated by red–blue- and grey-colored molecular surfaces, respectively.

The docking analysis results based on CG4 values and interactions comprising Conventional Hydrogen Bond: *CHB*, Van der Waals: *VdW*, Water Hydrogen Bond: *WHB*, Pi-Pi Stacked: *Pi-Pi S*, Carbon Hydrogen Bond: *CaHB*, Pi-Donor Hydrogen Bond: *Pi-DHB*; Alkyl: *A*; Pi-Alkyl: *Pi-A*; Halogen: *X*; an attractive charge/salt bridge; Pi-anion: *Pi-a*, Pi-Sigma: *Pi-s* for NPs–2RGU and NPs–2ONC complexes are given in Figures 10 and 11 and Table S9. Visual analysis of each docked NP revealed that all poses are located within the DPP-4 receptor-binding cavity. The high affinity for a receptor is conditioned by the number of rotatable bonds (RBN), the polarity, and the length of the ligand [72]. The selected NPs, with the best CG4 docking scores, displayed the same or greater RBN except for ZINC524732009, a similar length/size, and lower polarity than diabetes-approved drugs (Table 1), which could favor a longer interaction with the receptor. Furthermore, asymmetrical NP structures have numerous advantages because of their high affinity for receptor binding sites, which have both a non-polar region and a polar region, depicted in grey and red–blue, respectively (Figure 10). Hydrogen bonds with Ser630, Glu205, Glu206, Tyr631, Tyr547, HOH1041, and HOH 1020, hydrophobic interactions with Tyr547, Trp629, Phe357, Tyr666, and Tyr631, and electrostatic (Pi-anion) interactions with Glu206 and Arg669 were observed for the selected NPs.

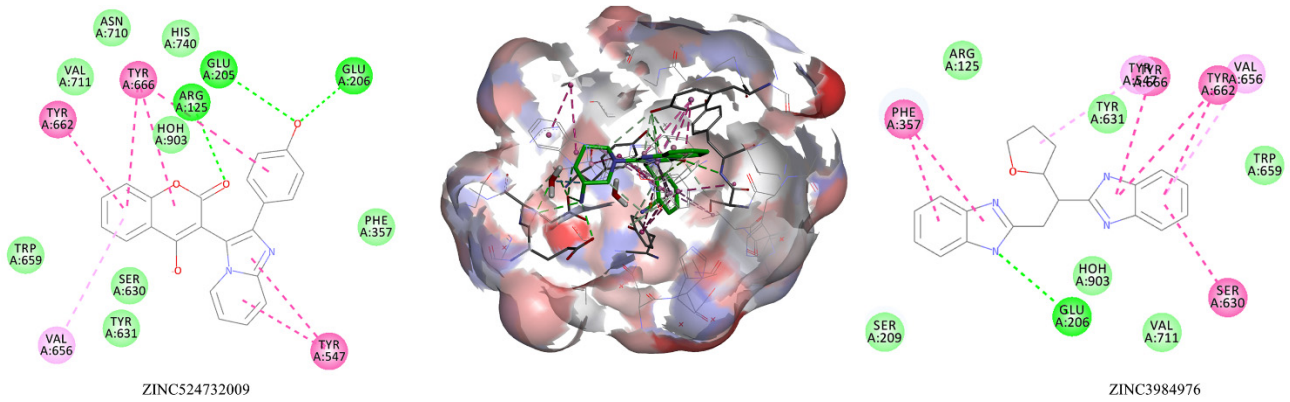

Figure 11. The two docked NPs in the 2ONC active site, showing a better CG4 score than alogliptin. Polar and non-polar regions of the binding site of 2RGU are illustrated by red–blue- and grey-colored molecular surfaces, respectively.

To sum up all docking observations (Figures 10 and 11 and Table S9), we can conclude that Glu205, Glu206, Tyr547, Ser630, Tyr 631, Tyr662, and Tyr666 are essential amino acid residues implicated in NPs–DPP-4 hydrogen bonding interactions. Likewise, hydrogen bonds with Arg358 and Asn710 for the ZINC12296449 NP were noticed. Moreover, all selected NPs were stabilized at the receptor-binding site by a considerable number of hydrophobic interactions, such as: *Amide-Pi Stacked* (Ser630, Tyr631), *Pi-Alkyl* (Phe357, Trp629, Tyr547, Tyr631, Tyr662, Try666, Val656), *Pi-Pi Stacked* (Phe357, Trp629, Tyr547, Tyr662, Tyr666), *Pi-Pi T-shaped* (Phe357, Tyr547, Tyr666), *Pi-Sigma* (Phe357, Trp629), *Halogen* (Glu206), and electrostatic interactions: *Attractive Charge* (Arg358), *Pi-Anion* (Glu206), *Salt Bridge* (Glue206, Arg358, Arg669). Together, these types of interactions (hydrogen bonds (*CHB*, *WHB*, *CaHB*, etc.), electrostatic, hydrophobic (*Pi-Pi S*, *Pi-a*, *Pi-A*, *Pi-s*, etc.)) play a crucial role in strengthening NPs–2RGU and NPs–2ONC complexes. The results presented in this paper are in accord with previously published papers [73–76].

Looking ahead, the NPs' docked poses were visualized with the CoSyM online tool (https://csm.ouproj.org.il/, accessed on 14 August 2022), and their continuous symmetry measurements (CSMs) were calculated (Table S10, Figure 12). The CSM delivers the distance of a structure from its perfect symmetry [77,78]. The delivered results give us information about how much symmetry is in a non-symmetric configuration (a value of zero of CSM represents perfect symmetry/achirality for a compound). The values greater than zero for Cn (the deviation from the nearest structure with rotational symmetry of order n (n = 2, 3, 4, . . . , 20)) and Sn (the deviation from the nearest structure with improper rotational symmetry of order n (n = 4, 6, 8, . . . , 20)) (Table S10) show the distance from their perfect symmetry for each docked pose of the NPs. The (x, y, z) values of the direction vector that describes the rotation axis on a reflection plane are also displayed in Table S10. In addition, the dipole moment (μ) for each NP was calculated using the density functional theory (DFT) with the Becke, three-parameter Lee–Yang–Parr (B3LYP) functional, and 6–31 G(d, p) basis sets, employing the Jaguar module of the Schrödinger package [79]. The values that are not zero for the dipole moment (Figure 12, Table S10) for each docked pose of the NPs are caused by their asymmetric structure [80] because the bond dipole moments do not cancel each other out [81].

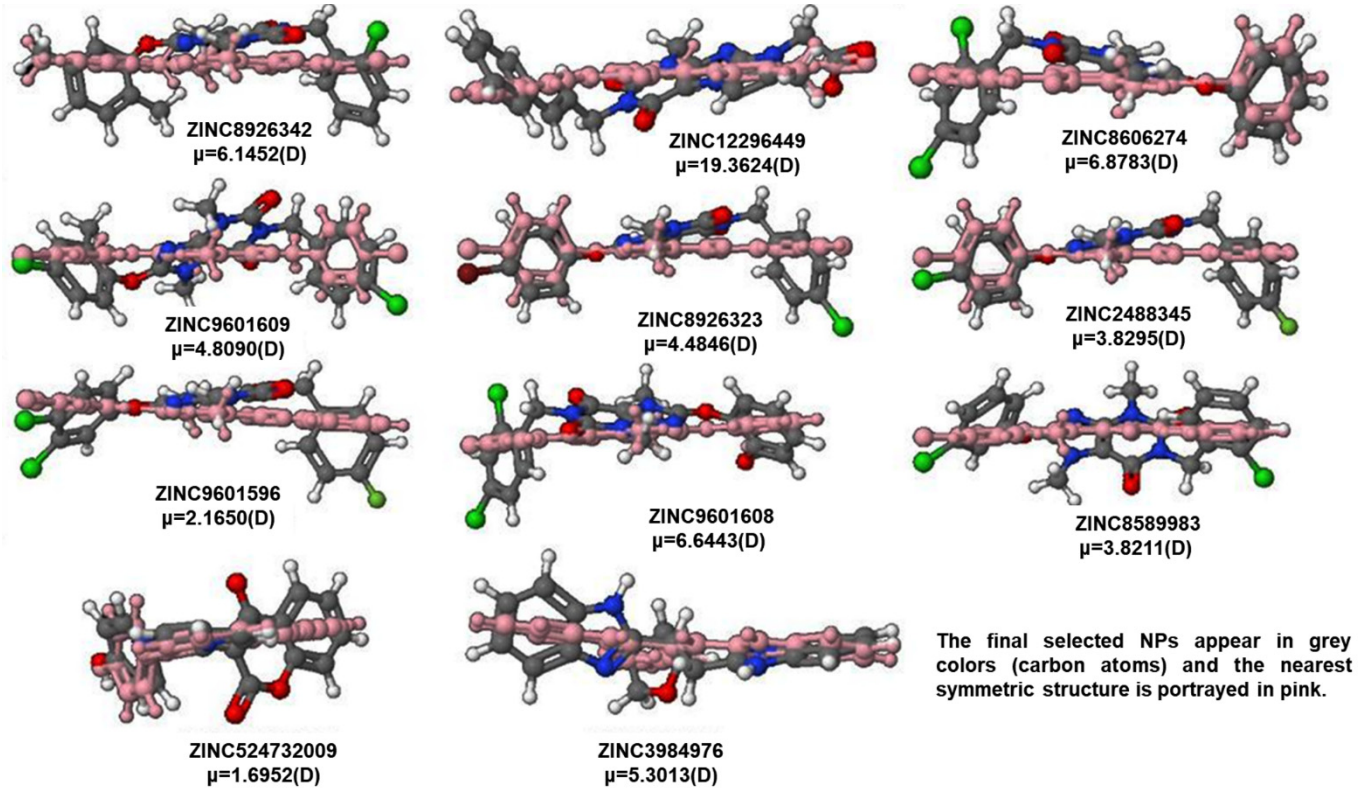

Figure 12. The docked pose of each selected NP overlaid across its nearest symmetric structure; the dipole moment (μ) is measured in Debye units (D).

The number of asymmetrical compounds exceeds the number of symmetrical ones, and their advantages or disadvantages in being used as active ingredients depend on the receptor pocket and possible interactions with it [82]. In general, asymmetrical molecules show a higher water solubility [83,84], which allows them to penetrate biological membranes and expand the chance to interact with the biological target. Therefore, asymmetrical compounds are interesting in terms of their structure, configuration, and bioavailability nature and deserve to be seen as an important "ingredient" in drug design and development.

4. Conclusions

DPP-4 is one of the essential targets to fight T2DM, with the gliptins class changing the idea of diabetes control for healthcare diabetes experts. Based on these realities, in silico scenarios involving 3D-shape virtual screening, molecular docking, and ADMETox predictions were performed to identify potential asymmetrical NPs from the ZINC-NPs DB that would be able to inhibit the DPP-4 target. Eleven asymmetrical NPs were demonstrated to be the most promising candidates in terms of both drug metabolism and safety profile. The molecular docking simulation revealed the binding modes of asymmetrical NPs in the active site of DPP-4. The present in silico outcomes strengthen the way of designing promising DPP-4 inhibitors from natural sources. To ensure the natural DPP-4 inhibitors' success, additional in vitro/in vivo experiments are required.

Supplementary Materials: The following supporting information can be downloaded at: https://www.mdpi.com/article/10.3390/sym14091842/s1, Table S1: The selected NPs by best 3D-similarity coefficients vs. linagliptin (Tanimoto Combo, TC > 1, ShapeTanimoto, ShT > 0.75, and Combo Score, CS > 1.2); Table S2: The selected NPs by best 3D-similarity coefficients vs. sitagliptin (Tanimoto Combo, TC > 1, ShapeTanimoto, ShT > 0.75, and Combo Score, CS > 1.2); Table S3: The selected NPs by best 3D-similarity coefficients vs. alogliptin (Tanimoto Combo, TC > 1, ShapeTanimoto, ShT > 0.75, and Combo Score, CS > 1.2); Table S4: 2D structures of selected NPs and docking score values; Table S5: Absorption parameters for selected NPs and drugs (pkCSM online tool was engaged); Table S6: Distribution parameters parameters for selected NPs and drugs (pkCSM online tool was engaged); Table S7: Metabolism and excretion parameters for selected NPs and drugs (pkCSM online tool was engaged); Table S8: Toxicity parameters for selected NPs and drugs (pkCSM online tool was engaged); Table S9: Docked interaction analysis of selected NP compounds with target proteins 2RGU and 2ONC; Table S10: The CSM values for the docked pose of each NP.

Author Contributions: Conceptualization, L.C. and D.I.; methodology, L.C.; validation, L.C. and D.I.; formal analysis, L.C. and D.I.; investigation, L.C. and D.I.; resources, L.C.; writing—original draft preparation, L.C. and D.I.; writing—review and editing, L.C.; visualization, L.C. and D.I.; supervision, L.C. All authors have read and agreed to the published version of the manuscript.

Funding: This research received no external funding. The APC was funded by L.C.

Institutional Review Board Statement: Not applicable.

Informed Consent Statement: Not applicable.

Data Availability Statement: Not applicable.

Acknowledgments: The authors thank Chemaxon Ltd. and OpenEye Ltd. for providing an academic license. Access to OpenEye Ltd. (https://www.eyesopen.com/) and BIOVIA Dassault Systèmes (for the Discovery Studio Visualizer) software is gratefully acknowledged by the authors. The authors would like to thank Ramona Curpan ("Coriolan Dragulescu" Institute of Chemistry) for providing access to Schrödinger software. This work was supported by Project No. 1.2 of the "Coriolan Dragulescu" Institute of Chemistry, Timisoara, Romania.

Conflicts of Interest: The authors declare that they have no conflict of interest.

Abbreviations

The following abbreviations are mentioned in this manuscript:

ADMETox	Absorption, distribution, metabolism, excretion, and toxicity;
BBB	Blood–brain barrier;
CS	Combo score;
DPP-4	Dipeptidyl peptidase 4;
EMA	European Medicines Agency;
HIA	Human gastrointestinal absorption;
IDF	International Diabetes Federation;
NPs	Natural products;
PDB	RCSB Protein Data Bank;
ShT	Shape Tanimoto;
TC	Tanimoto Combo;
T2DM	Type 2 diabetes mellitus;
ZINC-NPs DB	ZINC15 natural products database;
WHO	World Health Organization.

References

1. World Health Organization. Available online: Tps://www.who.int/health-topics/diabetes (accessed on 8 April 2022).
2. IDF Diabetes Atlas. Available online: http://www.idf.org/diabetesatlas (accessed on 8 April 2022).
3. Souto, S.B.; Souto, E.B.; Braga, D.C.; Medina, J.L. Prevention and current onset delay approaches of type 2 diabetes mellitus (T2DM). *Eur. J. Clin. Pharmacol.* **2011**, *67*, 653–661. [CrossRef] [PubMed]
4. Forbes, J.M.; Cooper, M.E. Mechanisms of diabetic complications. *Physiology* **2013**, *93*, 137–188. [CrossRef] [PubMed]
5. Weyer, C.; Bogardus, C.; Mott, D.M.; Pratley, R.E. The natural history of insulin secretory dysfunction and insulin resistance in the pathogenesis of type 2 diabetes mellitus. *J. Clin. Investig.* **1999**, *104*, 787–794. [CrossRef] [PubMed]
6. Crisan, L.; Pacureanu, L.; Avram, S.; Bora, A.; Avram, S.; Kurunczi, L. PLS and shape-based similarity analysis of maleimides–GSK-3 inhibitors. *J. Enzyme Inhib. Med. Chem.* **2014**, *29*, 599–610. [CrossRef]
7. Crisan, L.; Avram, S.; Pacureanu, L. Pharmacophore-based screening and drug repurposing exemplified on glycogen synthase kinase-3 inhibitors. *Mol. Divers.* **2017**, *21*, 385–405. [CrossRef]
8. Mulakayala, N.; Reddy, U.C.H.; Iqbal, J.; Pal, M. Synthesis of dipeptidyl peptidase-4 inhibitors: A brief overview. *Tetrahedron* **2010**, *66*, 4919–4938. [CrossRef]
9. Augustyns, K.; Van der Veken, P.; Senten, K.; Haerners, A. Dipeptidyl peptidase IV inhibitors as new therapeutic agents for the treatment of Type 2 diabetes. *Expert Opin. Ther. Patents* **2003**, *13*, 499–510. [CrossRef]
10. Wang, N.; Yang, T.; Li, J.; Zhang, X. Dipeptidyl peptidase-4 inhibitors as add-on therapy to insulin in patients with type 2 diabetes mellitus: A meta-analysis of randomized controlled trials. *Diabetes Metab. Syndr. Obes.* **2019**, *12*, 1513–1526. [CrossRef]
11. Seshadri, K.G.; Kirubha, M.H.B. Gliptins: A new class of oral antidiabetic agents. *Indian J. Pharm. Sci.* **2009**, *71*, 608–614. [CrossRef]
12. Gupta, V.; Kalra, S. Choosing a gliptin. *Indian J. Endocrinol. Metab.* **2011**, *15*, 298–308. [CrossRef]
13. PLoSker, G.L. Sitagliptin: A review of its use in patients with type 2 diabetes mellitus. *Drugs* **2014**, *74*, 223–242. [CrossRef] [PubMed]
14. Dhillon, S. Sitagliptin: A review of its use in the management of type 2 diabetes mellitus. *Drugs* **2010**, *70*, 489–512. [CrossRef]
15. Keating, G.M. Vildagliptin: A review of its use in type 2 diabetes mellitus. *Drugs* **2010**, *70*, 2089–2112. [CrossRef] [PubMed]
16. Dhillon, S. Saxagliptin: A Review in Type 2 Diabetes. *Drugs* **2015**, *75*, 1783–1796. [CrossRef]
17. Lajara, R. Use of the dipeptidyl peptidase-4 inhibitor linagliptin in combination therapy for type 2 diabetes. *Expert Opin. Pharmacother.* **2012**, *13*, 2663–2671. [CrossRef] [PubMed]
18. Keating, G.M. Alogliptin: A review of its use in patients with type 2 diabetes mellitus. *Drugs* **2015**, *75*, 777–796. [CrossRef] [PubMed]
19. Deeks, E.D. Linagliptin: A review of its use in the management of type 2 diabetes mellitus. *Drugs* **2012**, *72*, 1793–1824. [CrossRef]
20. Scott, L.J. Linagliptin in type 2 diabetes mellitus. *Drugs* **2011**, *71*, 611–624. [CrossRef]
21. Marino, A.B.; Cole, S.W. Alogliptin: Safety, efficacy, and clinical implications. *J. Pharm. Pract.* **2015**, *28*, 99–106. [CrossRef]
22. Saisho, Y. Alogliptin benzoate for management of type 2 diabetes. *Vasc. Health Risk. Manag.* **2015**, *11*, 229–243. [CrossRef]
23. Haak, T. Combination of Linagliptin and Metformin for the Treatment of Patients with Type 2 Diabetes. *Clin. Med. Insights Endocrinol. Diabetes* **2015**, *8*, 1–6. [CrossRef] [PubMed]
24. Takeshita, Y.; Kita, Y.; Kato, K.-I.; Kanamori, T.; Misu, H.; Kaneko, S.; Takamura, T. Effects of metformin and alogliptin on body composition in people with type 2 diabetes. *J. Diabetes. Investig.* **2019**, *10*, 723–730. [CrossRef] [PubMed]
25. Shinya, N.; Mariko, A.; Hiroyuki, I. Anagliptin in the treatment of type 2 diabetes: Safety, efficacy, and patient acceptability. *Metab. Syndrome Obes. Targets Ther.* **2015**, *8*, 163–171.
26. Kim, S.H.; Lee, S.H.; Yim, H.J. Gemigliptin, a novel dipeptidyl peptidase 4 inhibitor: First new anti-diabetic drug in the history of Korean pharmaceutical industry. *Arch. Pharm. Res.* **2013**, *36*, 1185–1188. [CrossRef]
27. Scott, L.J. Teneligliptin: A review in type 2 diabetes. *Clin. Drug Invest.* **2015**, *35*, 765–772. [CrossRef] [PubMed]
28. Mccormack, P.L. Evogliptin: First Global Approval. *Drugs* **2015**, *75*, 2045–2049. [CrossRef] [PubMed]
29. Biftu, T.; Sinha-Roy, R.; Chen, P.; Qian, X.; Feng, D.; Kuethe, J.T.; Scapin, G.; Gao, Y.D.; Yan, Y.; Krueger, D.; et al. Omarigliptin (MK-3102): A novel long-acting DPP-4 inhibitor for once-weekly treatment of type 2 diabetes. *J. Med. Chem.* **2014**, *57*, 3205–3212. [CrossRef]
30. Kaku, K. First novel once-weekly DPP-4 inhibitor, trelagliptin, for the treatment of type 2 diabetes mellitus. *Expert Opin. Pharmacother.* **2015**, *16*, 2539–2547. [CrossRef]
31. Sharma, R.; Sun, H.; Piotrowski, D.W.; Ryder, T.F.; Doran, S.D.; Dai, H.Q.; Prakash, C. Metabolism, excretion, and pharmacokinetics of (3,3-Diuoropyrrolidin1-yl)((2S,4S)-4-(4-(pyrimidin-2-yl)piperazin-1-yl)pyrrolidin-2-yl)methanone, a dipeptidyl peptidase inhibitor, in rat, dog and human. *Drug Metab. Dispos.* **2012**, *40*, 2143–2161. [CrossRef]
32. Crisan, L.; Pacureanu, L.; Bora, A.; Avram, S.; Kurunczi, L.; Simon, Z. QSAR study and molecular docking on indirubin inhibitors of Glycogen Synthase Kinase-3. *Cent. Eur. J. Chem.* **2013**, *11*, 63–67. [CrossRef]
33. Ivan, D.; Crisan, L.; Funar-Timofei, S.; Mracec, M. A quantitative structure–activity relationships study for the anti-HIV-1 activities of 1-[(2-hydroxyethoxy)methyl]-6-(phenylthio)thymine derivatives using the multiple linear regression and partial least squares methodologies. *J. Serb. Chem. Soc.* **2013**, *78*, 495–506. [CrossRef]
34. Petric, M.; Crisan, L.; Crisan, M.; Micle, A.; Maranescu, B.; Ilia, G. Synthesis and QSRR Study for a Series of Phosphoramidic Acid Derivatives. *Heteroat. Chem.* **2013**, *24*, 138–145. [CrossRef]

35. Rogic, S.; Nukic, M.; Gagic, Z. Quantitative Structure-Activity Relationship Study of DPP-4 Enzyme Inhibitors as Drugs in Therapy of Type 2 Diabetes Mellitus. International Conference on Medical and Biological Engineering, CMBEBIH 2021. In *CMBEBIH 2021*; Badnjevic, A., Gurbeta Pokvić, L., Eds.; Springer: Berlin/Heidelberg, Germany; Volume 84, pp. 481–488.
36. Upadhyay, J.; Gajjar, A.; Suhagia, B.N. Combined Ligand-Based and Structure-Based Virtual Screening Approach for Identification of New Dipeptidyl Peptidase 4 Inhibitors. *Curr. Drug Discov. Technol.* **2019**, *16*, 426–436. [CrossRef] [PubMed]
37. Rakesh, K.P.; Virendra, N.; Vipin, K. Structure based virtual screening of natural compounds and molecular dynamics simulation: Butirosin as Dipeptidyl peptidase (DPP-IV) inhibitor. *Biocat. Agricl. Biotech.* **2021**, *35*, 102042.
38. Wang, W.; Tian, Y.; Wan, Y.; Gu, S.; Ju, X.; Luo, X.; Liu, G. In silico studies of diarylpyridine derivatives as novel HIV-1 NNRTIs using docking-based 3D-QSAR, molecular dynamics, and pharmacophore modeling approaches. *RSC Adv.* **2018**, *8*, 40529–40543.
39. Gajjar, K.A.; Gajjar, A.K. Combiphore (Structure and Ligand Based Pharmacophore)—Approach for the Design of GPR40 Modulators in the Management of Diabetes. *Curr. Drug Discov. Technol.* **2020**, *17*, 233–247. [CrossRef]
40. Swilam, N.; Nawwar, M.A.M.; Radwan, R.A.; Mostaf, E.S. Antidiabetic Activity and In Silico Molecular Docking of Polyphenols from Ammannia baccifera L. subsp. Aegyptiaca (Willd.) Koehne Waste: Structure Elucidation of Undescribed Acylated Flavonol Diglucoside. *Plants* **2022**, *11*, 452. [CrossRef]
41. Pangajavalli, S.; Ranjithkumar, R.; Ramaswamy, S. Structural, Hirshfeld, spectroscopic, quantum chemical and molecular docking studies on 6b′, 7′, 8′, 9′-Tetrahydro-2H,6′H-spiro[acenaphthylene-1,11′-chromeno [3,4-a]pyrrolizine]-2,6′(6a′H,11a′H)-dione. *J. Mol. Struc.* **2020**, *1209*, 127921. [CrossRef]
42. Singh, P.; Singh, V.K.; Singh, A.K. Molecular docking analysis of candidate compounds derived from medicinal plants with type 2 diabetes mellitus targets. *Bioinformation* **2019**, *15*, 179–188. [CrossRef]
43. Crisan, L.; Borota, A.; Bora, A.; Pacureanu, L. Diarylthiazole and diarylimidazole selective COX-1 inhibitor analysis through pharmacophore modeling, virtual screening, and DFT-based approaches. *Struct. Chem.* **2019**, *30*, 2311–2326. [CrossRef]
44. Visa, A.; Maranescu, B.; Lupa, L.; Crisan, L.; Borota, A. New Efficient Adsorbent Materials for the Removal of Cd(II) from Aqueous Solutions. *Nanomaterials* **2020**, *10*, 899. [CrossRef]
45. Jabeen, E.; Janjua, N.K.; Ahmed, S.; Murtaza, I.; Ali, T.; Masood, N.; Rizvi, A.S.; Murtaza, G. DFT predictions, synthesis, stoichiometric structures and anti-diabetic activity of Cu (II) and Fe (III) complexes of quercetin, morin, and primuletin. *J. Mol. Struc.* **2017**, *1150*, 459–468. [CrossRef]
46. Visa, A.; Mracec, M.; Maranescu, B.; Maranescu, V.; Ilia, G.; Popa, A.; Mracec, M. Structure simulation into a lamellar supramolecular network and calculation of the metal ions/ligands ratio. *Chem. Cent. J.* **2012**, *6*, 91. [CrossRef] [PubMed]
47. Meduru, H.; Wang, Y.-T.; Tsai, J.J.P.; Chen, Y.-C. Finding a Potential Dipeptidyl Peptidase-4 (DPP-4) Inhibitor for Type-2 Diabetes Treatment Based on Molecular Docking, Pharmacophore Generation, and Molecular Dynamics Simulation. *Int. J. Mol. Sci.* **2016**, *17*, 920. [CrossRef]
48. Hidalgo-Figueroa, S.; Rodríguez-Luévano, A.; Almanza-Pérez, J.C.; Giacoman-Martínez, A.; Ortiz-Andrade, R.; León-Rivera, I.; Navarrete-Vázquez, G. Synthesis, molecular docking, dynamic simulation and pharmacological characterization of potent multifunctional agent (dual GPR40-PPARγ agonist) for the treatment of experimental type 2 diabetes. *Eur. J. Pharmacol.* **2021**, *907*, 174244. [CrossRef] [PubMed]
49. *ROCS, v. 3.5.0.1*; OpenEye Scientific Software Inc.: Santa Fe, NM, USA, 2021.
50. *FRED, v.4.1.2.1*; OpenEye Scientific Software Inc.: Santa Fe, NM, USA, 2021.
51. BIOVIA. *Discovery Studio Visualizer v. 20.1.0*; Accelrys Software Inc.: San Diego, CA, USA, 2020.
52. Daina, A.; Michielin, O.; Zoete, V. SwissADME: A free web tool to evaluate pharmacokinetics, drug-likeness and medicinal chemistry friendliness of small molecules. *Sci. Rep.* **2017**, *7*, 42717. [CrossRef]
53. Pires, D.E.V.; Blundell, T.L.; Ascher, D.B. pkCSM: Predicting Small-Molecule Pharmacokinetic and Toxicity Properties Using Graph-Based Signatures. *J. Med. Chem.* **2015**, *58*, 4066–4072. [CrossRef]
54. Sterling, T.; Irwin, J.J. ZINC 15—Ligand Discovery for Everyone. *J. Chem. Inf. Model.* **2015**, *55*, 2324–2337. [CrossRef]
55. Crisan, L.; Bora, A. Small Molecules of Natural Origin as Potential Anti-HIV Agents: A Computational Approach. *Life* **2021**, *11*, 722. [CrossRef]
56. *Schrödinger Release 2021-4: LigPrep (2021) Schrödinger*; LLC: New York, NY, USA, 2021.
57. Hawkins, P.C.D.; Skillman, A.G.; Warren, G.L.; Ellingson, B.A.; Stahl, M.T. Conformer Generation with OMEGA: Algorithm and Validation Using High Quality Structures from the Protein Databank and Cambridge Structural Database. *J. Chem. Inf. Model.* **2010**, *50*, 572–584. [CrossRef]
58. Thom, R.; Löffler, B.; Stihle, M.; Huber, W.; Ruf, A.; Hennig, M. Structural Basis of Proline-Specific Exopeptidase Activity as Observed in Human Dipeptidyl Peptidase-IV. *Structure* **2003**, *11*, 947–959. [CrossRef]
59. Brown, J.H. Breaking symmetry in protein dimers: Designs and functions. *Protein Sci.* **2006**, *15*, 1–13. [CrossRef] [PubMed]
60. Kim, D.; Wang, L.; Beconi, M.; Eiermann, G.J.; Fisher, M.H.; He, H.; Hickey, G.J.; Kowalchick, J.E.; Leiting, B.; Lyons, K.; et al. (2*R*)-4-Oxo-4-[3-(Trifluoromethyl)-5,6-dihydro[1,2,4]triazolo[4,3-*a*]pyrazin-7(8*H*)-yl]-1-(2,4,5-trifluorophenyl)butan-2-amine: A Potent, Orally Active Dipeptidyl Peptidase IV Inhibitor for the Treatment of Type 2 Diabetes. *J. Med. Chem.* **2005**, *48*, 141–151. [CrossRef]

61. Eckhardt, M.; Langkopf, E.; Mark, M.; Tadayyon, M.; Thomas, L.; Nar, H.; Pfrengle, W.; Guth, B.; Lotz, R.; Sieger, P.; et al. 8-(3-(R)-Aminopiperidin-1-yl)-7-but-2-ynyl-3-methyl-1-(4-methyl-quinazolin-2-ylmethyl)-3,7-dihydropurine-2,6-dione (BI 1356), a Highly Potent, Selective, Long-Acting, and Orally Bioavailable DPP-4 Inhibitor for the Treatment of Type 2 Diabetes. *J. Med. Chem.* **2007**, *50*, 6450–6453. [CrossRef] [PubMed]
62. Feng, J.; Zhang, Z.; Wallace, M.B.; Stafford, J.A.; Kaldor, S.W.; Kassel, D.B.; Navre, M.; Shi, L.; Skene, R.J.; Asakawa, T.; et al. Discovery of Alogliptin: A Potent, Selective, Bioavailable, and Efficacious Inhibitor of Dipeptidyl Peptidase IV. *J. Med. Chem.* **2007**, *50*, 2297–2300. [CrossRef]
63. *MakeReceptor, v. 3.5.0.4*; OpenEye Scientific Software Inc.: Santa Fe, NM, USA, 2020.
64. *Schrödinger Release 2021-4: Maestro, v.13.0.135 (2021) Schrödinger*; LLC: New York, NY, USA, 2021.
65. Lipinski, C.A.; Lombardo, F.; Dominy, B.W.; Feeney, P.J. Experimental and computational approaches to estimate solubility and permeability in drug discovery and development settings. *Adv. Drug Deliv. Rev.* **1997**, *23*, 3–25. [CrossRef]
66. Jorgensen, W.L.; Duffy, E.M. Prediction of drug solubility from structure. *Adv. Drug Deliv. Rev.* **2002**, *54*, 355–366. [CrossRef]
67. Hanley, J.A.; McNeil, B.J. The meaning and use of the area under a receiver operating characteristic (ROC) curve. *Radiology* **1982**, *143*, 29–36. [CrossRef]
68. Avram, S.I.; Pacureanu, L.M.; Bora, A.; Crisan, L.; Avram, S.; Kurunczi, L. ColBioSFlavRC: A Collection of Bioselective Flavonoids and Related Compounds Filtered from HighThroughput Screening Outcomes. *J. Chem. Inf. Model.* **2014**, *54*, 2360–2370. [CrossRef]
69. Mysinger, M.M.; Carchia, M.; Irwin, J.J.; Shoichet, B.K. Directory of useful decoys, enhanced (DUD-E): Better ligands and decoys for better benchmarking. *J. Med. Chem.* **2012**, *26*, 6582–6594. [CrossRef]
70. Giangreco, I.; Mukhopadhyay, A.; Cole, J.C. Validation of a Field-Based Ligand Screener Using a Novel Benchmarking Data Set for Assessing 3D-Based Virtual Screening Methods. *J. Chem. Inf. Model.* **2021**, *61*, 5841–5852. [CrossRef] [PubMed]
71. Jain, A.N.; Nicholls, A. Recommendations for evaluation of computational methods. *J. Comput. Aided. Mol. Des.* **2008**, *22*, 133–139. [CrossRef] [PubMed]
72. Filisola-Villaseñor, J.G.; Aranda-Barradas, M.E.; Miranda-Castro, S.P.; Mendieta-Wejebe, J.E.; Valdez Guerrero, A.S.; Guillen Castro, S.A.; Martínez Castillo, M.; Tamay-Cach, F.; Álvarez-Almazán, S. Impact of Molecular Symmetry/Asymmetry on Insulin-Sensitizing Treatments for Type 2 Diabetes. *Symmetry* **2022**, *14*, 1240. [CrossRef]
73. Sever, B.; Soybir, H.; Görgülü, Ş.; Cantürk, Z.; Altıntop, M.D. Pyrazole Incorporated New Thiosemicarbazones: Design, Synthesis and Investigation of DPP-4 Inhibitory Effects. *Molecules* **2020**, *25*, 5003. [CrossRef] [PubMed]
74. Yoshida, T.; Akahoshi, F.; Sakashita, H.; Kitajima, H.; Nakamura, M.; Sonda, S.; Takeuchi, M.; Tanaka, Y.; Ueda, N.; Sekiguchi, S.; et al. Discovery and preclinical profile of teneligliptin (3-[(2S,4S)-4-[4-(3-methyl1-phenyl-1H-pyrazol-5-yl)piperazin-1-yl]pyrrolidin-2- ylcarbonyl]thiazolidine): A highly potent, selective, long-lasting and orally active dipeptidyl peptidase IV inhibitor for the treatment of type 2 diabetes. *Bioorg. Med. Chem.* **2012**, *20*, 5705–5719. [PubMed]
75. Pantaleão, S.Q.; Maltarollo, V.G.; Araujo, S.C.; Gertrudes, J.C.; Honorio, K.M. Molecular docking studies and 2D analyses of DPP-4 inhibitors as candidates in the treatment of diabetes. *Mol. Biosyst.* **2015**, *11*, 3188–3193. [CrossRef]
76. Pan, J.; Zhang, Q.; Zhang, C.; Yang, W.; Liu, H.; Lv, Z.; Liu, J.; Jiao, Z. Inhibition of Dipeptidyl Peptidase-4 by Flavonoids: Structure-Activity Relationship, Kinetics and Interaction Mechanism. *Front Nutr.* **2022**, *12*, 892426. [CrossRef] [PubMed]
77. Alon, G.; Tuvi-Arad, I. Improved algorithms for symmetry analysis: Structure preserving permutations. *J. Math. Chem.* **2018**, *56*, 193–212. [CrossRef]
78. Zabrodsky, H.; Peleg, S.; Avnir, D. Continuous symmetry measures. *J. Am. Chem. Soc.* **1992**, *114*, 7843–7851. [CrossRef]
79. Bochevarov, A.D.; Harder, E.; Hughes, T.F.; Greenwood, J.R.; Braden, D.A.; Philipp, D.M.; Rinaldo, D.; Halls, M.D.; Zhang, J.; Friesner, R.A. Jaguar: A high-performance quantum chemistry software program with strengths in life and materials sciences. *Int. J. Quantum Chem.* **2013**, *113*, 2110–2142. [CrossRef]
80. Li, D.; Wang, B.; Long, X.; Xu, W.; Xia, Y.; Yang, D.; Yao, X. Controlled Asymmetric Charge Distribution of Active Centers in Conjugated Polymers for Oxygen Reduction. *Angew. Chem.* **2021**, *60*, 26483–26488. [CrossRef] [PubMed]
81. Tripathy, T.; De, B.R. Making sense about Dipole Moments. *J. Phys. Sci.* **2008**, *12*, 155–172.
82. Álvarez-Almazán, S.; Filisola-Villaseñor, J.G.; Alemán-González-Duhart, D.; Tamay-Cach, F.; Mendieta-Wejebe, J.E. Current molecular aspects in the development and treatment of diabetes. *J. Physiol. Biochem.* **2020**, *76*, 13–35. [CrossRef] [PubMed]
83. Morimoto, J.; Miyamoto, K.; Ichikawa, Y.; Uchiyama, M.; Makishima, M.; Hashimoto, Y.; Ishikawa, M. Improvement in aqueous solubility of achiral symmetric cyclofenil by modification to a chiral asymmetric analog. *Sci. Rep.* **2021**, *11*, 12697. [CrossRef] [PubMed]
84. Veber, D.F.; Johnson, S.R.; Cheng, H.Y.; Smith, B.R.; Ward, K.W.; Kopple, K.D. Molecular properties that influence the oral bioavailability of drug candidates. *J. Med. Chem.* **2002**, *45*, 2615–2623. [CrossRef] [PubMed]